# A Reference-Free Molecular Feedback Controller for Inducing Sustained Oscillations in Gene Regulatory Networks

Frank Britto Bisso[1,+], Sergio Rengifo-Lozano[2,+], Subham Dey[3,+], Guy-Bart Stan[4], Christian Cuba Samaniego[1,*]

***Abstract*— Periodic behavior is a widespread biological phenomenon that occurs on multiple spatiotemporal scales, where upstream stimuli are encoded into dynamic intracellular signals. Restoring rhythmic dynamics after perturbations, or inducing them in otherwise steady-state systems, typically requires redesigning the underlying network, limiting scalability. Here we propose a reference-free molecular feedback controller built from the Incoherent Feedforward Loop (IFFL) motif that destabilizes the steady state of a non-oscillating system into sustained oscillations. We apply the controller to a self-inhibiting gene and show, through a Hopf bifurcation analysis, that sustained oscillations are induced in the fast sequestration regime when the indirect production branch of the IFFL motif dominates the direct one, and the actuation gain is sufficiently large relative to the process. Numerical simulations validate these conditions and characterize the robustness of the resulting oscillations, revealing that the period is robust to parametric perturbations while the amplitude is sensitive. Ultimately, we explore whether the same IFFL architecture extends to higher-dimensional processes by applying it, as a case study, to a negative feedback system in its non-oscillatory regime.**

**Keywords:** Incoherent Feedforward Loop (IFFL), Molecular controllers, Biological systems, Genetic Oscillator.

## I. Introduction

Periodic behavior is ubiquitous in biological systems across different spatiotemporal scales, as cellular function often requires regulators to oscillate with precise timing, duration, and amplitude [1]. Although the mechanisms underlying this regulation are not fully understood, disruptions to periodicity have been correlated with several disease phenotypes. For instance, loss of circadian oscillation amplitude is associated with neurodegenerative disorders [2], while altered clock gene timing promotes cancer progression [3].

In applied biotechnology, inducing sustained oscillations in otherwise non-oscillatory systems has been shown to increase bioproduction yield [4] and extend cellular lifespan in yeast [5]. Overall, whether the goal is to restore lost oscillations or to induce new ones, the proposed strategy is the same: the *de novo* design of a genetic oscillator. However, this approach is circuit-specific, meaning that the oscillatory conditions depend on the architecture and parameters of each particular network, and must be re-calculated or re-tuned when the oscillator is connected to a different downstream process [6], which limits scalability across biological applications.

Here, we propose an alternative strategy. Rather than engineering oscillatory dynamics within a gene regulatory network, we design an exogenous molecular feedback controller based on the Incoherent Feedforward Loop (IFFL) motif and molecular sequestration that destabilizes the steady state of a non-oscillating system into sustained oscillations, without requiring a predefined reference signal or redesign of the target network. In contrast to prior IFFL- and sequestration-based molecular controllers, which have primarily implemented robust perfect adaptation [7], [8], we use these primitives for the inverse control objective: reference-free destabilization of a stable equilibrium. To this end, we derive sufficient conditions for sustained oscillations in the fast sequestration regime through a Hopf bifurcation analysis, validate them numerically, and characterize the robustness of the resulting oscillations to parametric perturbations. We then explore whether the same IFFL architecture extends to higher-dimensional processes by applying it, as a case study, to a negative-feedback system, and ultimately discuss the biological feasibility of our design.

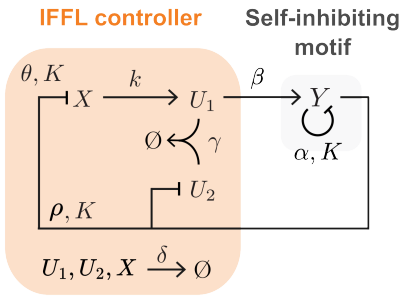


Fig. 1. **Reference-free molecular feedback controller.** The schematic of the chemical species that comprise the feedback controller are shown in orange, whereas the ones that describe the self-inhibiting gene are shown in gray.

## II. Results

Throughout this paper, we indicate chemical species with capital letters (e.g $U$) and their corresponding concentration with the corresponding lowercase letter (e.g $u$).

[1] Computational Biology Department, Carnegie Mellon University, Pittsburgh, PA 15213, USA. fbrittob@andrew.cmu.edu, ccubasam@andrew.cmu.edu
[2] National University of Trujillo, Trujillo, La Libertad, Peru. p880301324@unitru.edu.pe
[3] Center for Perceptual Systems, University of Texas at Austin, Austin, TX 78712, USA. subhamdey9983@gmail.com
[4] Department of Bioengineering, Imperial College London, UK. g.stan@imperial.ac.uk
[+] Authors contributed equally. [*] Corresponding author.

### A. Building the reference-free feedback controller

The molecular design of the proposed controller is based on the IFFL motif [9]. This motif processes the input $Y$ and upregulates the production of the species $U_2$ and $X$ with rate constants $\rho$ and $\theta$, respectively. Then, the $X$ species produces $U_1$ at rate constant $k$. Likewise, $U_2$ and $U_1$ interact via a sequestration mechanism at rate constant $\gamma$. Finally, we assume that every species decays at rate $\delta$. We can describe the network through the following chemical reactions:

$$\begin{aligned} &X \xrightarrow{k} X + U_1, \quad Y \xrightarrow{\rho} Y + U_2, && \text{Production,} \\ &Y \xrightarrow{\theta} Y + X, \quad X \xrightarrow{\delta} \emptyset, && \text{Production/Decay,} \\ &U_1 + U_2 \xrightarrow{\gamma} \emptyset, \quad U_1, U_2 \xrightarrow{\delta} \emptyset, && \text{Sequestration/Decay.} \end{aligned} \tag{1}$$

Furthermore, we consider a self-inhibiting gene as the process, while neglecting transcriptional, translational, and downstream delays, leading to non-oscillatory behavior. The gene produces a repressor $Y$, which downregulates its own expression with rate constant $\alpha p$ and degrades at rate $\delta$. The system is modeled by the following chemical reactions:

$$\emptyset \xrightarrow{\alpha p} Y, \quad Y \xrightarrow{\delta} \emptyset. \quad \text{Production/Decay} \tag{2}$$

where $p = \frac{K^m}{K^m + y^m}$. The IFFL controller couples to this process through the following chemical reactions:

$$U_1 \xrightarrow{\beta} U_1 + Y. \quad \text{Controller actuation} \tag{3}$$

Then, our goal with the controller is to destabilize the steady-state behavior of this system into sustained oscillations.

The closed-loop system, shown in Fig. 1 and written considering the $Y$ repressor in Eq. (2) as the input in Eq. (1), can be modeled using Ordinary Differential Equations (ODEs) following the law of mass action. We further consider a non-dimensionalized set of ODEs derived from the following change of variables: $\tau = \delta t, \hat{y} = \frac{y}{K}, \hat{u}_1 = \frac{u_1}{K}, \hat{u}_2 = \frac{u_2}{K}, \hat{x} = \frac{x}{K}$ and parameters $\hat{\alpha} = \frac{\alpha}{\delta K}, \hat{\beta} = \frac{\beta}{\delta}, \hat{k} = \frac{k}{\delta}.\hat{\gamma} = \frac{\gamma K}{\delta}, \hat{\rho} = \frac{\rho}{\delta K}, \hat{\theta} = \frac{\theta}{\delta K}$. The following ODEs describe our non-dimensionalized model:

$$\frac{d}{d\tau}\hat{u}_1 = \hat{k}\hat{x} - \hat{u}_1 - \hat{\gamma}\hat{u}_1\hat{u}_2 \tag{4}$$

$$\frac{d}{d\tau}\hat{u}_2 = \hat{\rho}\frac{1}{1+\hat{y}^m} - \hat{u}_2 - \hat{\gamma}\hat{u}_1\hat{u}_2 \tag{5}$$

$$\frac{d}{d\tau}\hat{x} = \hat{\theta}\frac{1}{1+\hat{y}^m} - \hat{x} \tag{6}$$

$$\frac{d}{d\tau}\hat{y} = \hat{\alpha}\frac{1}{1+\hat{y}^m} - \hat{y} + \hat{\beta}\hat{u}_1 \tag{7}$$

### B. Deriving the oscillatory condition

To outline the conditions under which the reference-free controller induces oscillations in the self-inhibiting gene, we start by showing that the closed-loop system described by Eqs. (4)-(7) is bounded. Then, in the fast sequestration regime ($\hat{\gamma} \to \infty$), we reduce the 4D system into a tractable lower-dimensional system, and identify the parametric regime in which this reduced system governs the closed-loop behavior. Ultimately, we perform a Hopf bifurcation analysis on the reduced system to derive the conditions under which the unique equilibrium loses stability. Since the trajectories are bounded and the equilibrium is unique, its instability implies the emergence of oscillations in the neighborhood of the bifurcation. We verified the persistence of such through numerical simulations, and provide insight into the biological feasibility of the design.

#### 1) Boundedness and steady-state analysis

In this subsection, we show that the closed-loop system admits a unique steady state, and that the corresponding trajectories are bounded. Since the Hill term satisfies $(1 + \hat{y}^m)^{-1} \leq 1$ and the sequestration term $\hat{\gamma}\hat{u}_1\hat{u}_2 > 0$, the right-hand sides of Eqs. (4)–(7) are bounded above, following the same approach as [10], by

$$\frac{d}{d\tau}\hat{u}_1 < \hat{k}\hat{\theta} - \hat{u}_1, \qquad \frac{d}{d\tau}\hat{u}_2 < \hat{\rho} - \hat{u}_2, \tag{8}$$

$$\frac{d}{d\tau}\hat{x} < \hat{\theta} - \hat{x}, \qquad \frac{d}{d\tau}\hat{y} < \hat{\alpha} + \hat{\beta}\hat{k}\hat{\theta} - \hat{y}. \tag{9}$$

Hence, the closed-loop trajectories are bounded for all $\tau \geq 0$. Furthermore, the controller nullcline $N_1$ is obtained by setting Eqs. (4)–(6) to zero, which yields

$$\bar{u}_2 = \frac{p_1 - \bar{u}_1}{\bar{u}_1} = \frac{p_2}{\bar{u}_1 + 1/\hat{\gamma}}, \tag{10}$$

where $p_1 = \hat{k}\hat{\theta}y^*$, $p_2 = \hat{\rho}y^*$, and $y^* = (1 + \bar{y}^m)^{-1}$. Here $\bar{u}_1$, $\bar{u}_2$, and $\bar{y}$ denote steady-state values of $\hat{u}_1$, $\hat{u}_2$, and $\hat{y}$, respectively. We note that Eq. (10) yields a quadratic in $\bar{u}_1$,

$$\bar{u}_1^2 + \left((p_2 - p_1) + \frac{1}{\hat{\gamma}}\right)\bar{u}_1 - \frac{p_1}{\hat{\gamma}} = 0. \tag{11}$$

Letting $\hat{r} = \hat{\rho}/(\hat{k}\hat{\theta})$ denote the ratio between the delayed and direct branches of the IFFL motif (Fig. 1, left), we have $p_1 - p_2 = \hat{k}\hat{\theta}(1 - \hat{r})y^*$. The unique non-negative root of Eq. (11) is

$$N_1 = \frac{1}{2}\left(p_1 - p_2 - \frac{1}{\hat{\gamma}} + \sqrt{\left(p_2 - p_1 + \frac{1}{\hat{\gamma}}\right)^2 + \frac{4p_1}{\hat{\gamma}}}\right) \tag{12}$$

In the fast-sequestration regime ($\hat{\gamma} \to \infty$), $N_1$ asymptotically approaches $\max\left(0, \hat{k}\hat{\theta}(1 - \hat{r})y^*\right)$, which is strictly positive for $\hat{r} < 1$. For $\hat{r} > 1$, the controller exerts no action on the process. At $\hat{r} = 1$, $N_1$ remains strictly positive for any finite $\hat{\gamma}$, since $N_1 \approx \sqrt{\hat{k}\hat{\theta}y^*/\hat{\gamma}} > 0$. Moreover, the process nullcline $N_2$ follows from setting Eq. (7) to zero:

$$N_2 = \frac{1}{\hat{\beta}}\bar{y} - \frac{\hat{\alpha}}{\hat{\beta}}\frac{1}{1 + \bar{y}^m}. \tag{13}$$

As shown in Appendices A and B, $N_1$ is monotonically decreasing in $\hat{y}$ for $\hat{r} < 1$ and $N_2$ is monotonically increasing, independently of $\hat{r}$. Since a strictly decreasing and a strictly increasing continuous curve cross at most once, and both are finite for all $\hat{y} \geq 0$, the nullclines intersect exactly once. Hence, for zero initial conditions and $\hat{r} \leq 1$, the closed-loop system admits a unique equilibrium.

*2) Dynamics in the fast sequestration regime*

To obtain a tractable description of the closed-loop dynamics, we exploit the fast-sequestration regime ($\hat{\gamma} \to \infty$), representing the tight binding observed in vivo between sigma/anti-sigma factor pairs [11], dimeric transcription factors [12], among others. Since the remaining terms in Eqs. (4)–(5) are bounded (Section B.1), the product $\hat{\gamma}\hat{u}_1\hat{u}_2$ can remain finite only if $\hat{u}_1\hat{u}_2 \to 0$. The fast-sequestration limit therefore confines the dynamics to the set $\{\hat{u}_1\hat{u}_2 = 0\}$. This constraint partitions the reachable state space into three cases, depending on which sequestration species is depleted:

$$S_1 = \{\hat{u}_1 = 0,\ \hat{u}_2 > 0\},$$
$$S_2 = \{\hat{u}_2 = 0,\ \hat{u}_1 > 0\},$$
$$S_3 = \{\hat{u}_1 = \hat{u}_2 = 0\}.$$

On each case, the closed-loop system reduces to a lower-dimensional set of ODEs obtained by setting the depleted variable(s) to zero in Eqs. (4)–(7).

*3) Identifying the partition that enables oscillations*

We now determine which of the three cases identified in Section B.2 can support oscillations, and under what parametric conditions the closed-loop trajectory occupies them.

On $S_3$, both controller species vanish ($\hat{u}_1 = \hat{u}_2 = 0$) and the closed-loop system reduces to a self-inhibiting gene without delay, which cannot undergo a Hopf bifurcation [13]. On $S_1$ ($\hat{u}_1 = 0$), the non-zero controller species $\hat{u}_2$ is drive by $\hat{y}$ through Eq. (5) but does not actuate the process. Then, the controller is effectively decoupled, and the closed-loop dynamics reduce to the same non-oscillatory subsystem found in $S_3$. The only remaining candidate is $S_2$ ($\hat{u}_2 = 0$), where the non-zero species $\hat{u}_1$ actuates the process through the term $\hat{\beta}\hat{u}_1$ in Eq. (7). This is the only feedback structure in the reduced dynamics capable of generating a Hopf bifurcation, which we analyze in Section B.4.

Having established that oscillations are possible only on $S_2$, we now determine the conditions under which the trajectory occupies this partition. We define the variable $z = \hat{u}_1 - \hat{u}_2$, whose sign determines which sequestration species is non-zero. Subtracting Eq. (5) from Eq. (4), and noting that the sequestration term enters both equations with identical coefficient and sign and therefore cancels, yields

$$\dot{z} + z = \Delta(\hat{x}, \hat{y}), \qquad \Delta = \hat{k}\hat{x} - \hat{\rho}(1 + \hat{y}^m)^{-1}. \tag{14}$$

The forcing term $\Delta$ determines the steady-state sign of $z$: $\Delta > 0$ drives $\hat{u}_1 > \hat{u}_2$, placing the trajectory on $S_2$, while $\Delta < 0$ drives the converse. Since the dynamics of $\hat{x}$ are linear and first-order (Eq. (6)), $\hat{x}$ rapidly approaches its nullcline, $\bar{x} = \hat{\theta}(1 + \hat{y}^m)^{-1}$. Evaluating $\Delta$ on this manifold gives

$$\Delta = \hat{k}\hat{\theta}(1 - \hat{r})(1 + \hat{y}^m)^{-1}, \tag{15}$$

where $\hat{r}$ denotes the ratio introduced in Section B.1. Since $(1 + \hat{y}^m)^{-1} > 0$, the sign of $\Delta$ is determined entirely by $1 - \hat{r}$. Therefore, the trajectory is driven onto the oscillatory branch $S_2$ if and only if $\hat{r} < 1$ At the boundary $\hat{r} = 1$, $\Delta$ vanishes and both controller species $\hat{u}_1$ and $\hat{u}_2$ remain small but finite at equilibrium, so the trajectory lies at the $S_1/S_2$ boundary rather than strictly inside $S_2$. Numerical simulations in Section II.C show that oscillations persist at $\hat{r} = 1$. We therefore state the design rule as $\hat{r} \leq 1$.

*4) Hopf bifurcation analysis*

On $S_2$ ($\hat{u}_2 = 0$), the sequestration term in the $\hat{u}_1$ equation vanishes and the closed-loop dynamics reduce to the three-dimensional system

$$\frac{d\hat{u}_1}{d\tau} = \hat{k}\hat{x} - \hat{u}_1, \tag{16}$$
$$\frac{d\hat{x}}{d\tau} = \hat{\theta}\,(1 + \hat{y}^m)^{-1} - \hat{x}, \tag{17}$$
$$\frac{d\hat{y}}{d\tau} = \hat{\alpha}\,(1 + \hat{y}^m)^{-1} - \hat{y} + \hat{\beta}\hat{u}_1. \tag{18}$$

Linearizing about the unique equilibrium $(\bar{u}_1, \bar{x}, \bar{y})$ of Section B.1 gives the Jacobian

$$J_{S_2} = \begin{bmatrix} -1 & \hat{k} & 0 \\ 0 & -1 & -\hat{\theta}\,h \\ \hat{\beta} & 0 & -1 - \hat{\alpha}\,h \end{bmatrix}, \tag{19}$$

where $h = h(\bar{y}) = m\bar{y}^{m-1}/(1 + \bar{y}^m)^2 > 0$. The associated characteristic polynomial is the cubic

$$P_{S_2}(s) = s^3 + a_2 s^2 + a_1 s + a_0, \tag{20}$$

with the following coefficients:

$$a_2 = 3 + \hat{\alpha}h, \qquad a_1 = 3 + 2\hat{\alpha}h, \qquad a_0 = 1 + \hat{\alpha}h + \hat{\beta}\hat{k}\hat{\theta}\,h. \tag{21}$$

All three coefficients $a_2$, $a_1$, $a_0$ are strictly positive, since $h > 0$ and all kinetic rates are non-negative. Stability of the equilibrium is then determined by the Routh–Hurwitz array of the cubic $P_{S_2}(s)$:

$$\begin{array}{c|cc} s^3 & 1 & a_1 \\ s^2 & a_2 & a_0 \\ s^1 & b_1 & 0 \\ s^0 & a_0 & 0 \end{array} \qquad b_1 = \frac{a_1 a_2 - a_0}{a_2}. \tag{22}$$

The equilibrium is asymptotically stable if and only if every entry of the first column is positive. We note that the entries 1, $a_2$, and $a_0$ are already positive, so stability is governed by the sign of $b_1$. Since $a_2 > 0$, this reduces to the sign of $a_1 a_2 - a_0$. At the boundary $b_1 = 0$, a complex-conjugate pair of eigenvalues lies on the imaginary axis, which marks a Hopf bifurcation,

$$a_1 a_2 = a_0. \tag{23}$$

Substituting the coefficients into Eq. (23),

$$(3 + 2\hat{\alpha}h)(3 + \hat{\alpha}h) = 1 + \hat{\alpha}h + \hat{\beta}\hat{k}\hat{\theta}\,h. \tag{24}$$

Expanding the left-hand side gives $2(\hat{\alpha}h)^2 + 9\hat{\alpha}h + 9$, so the Hopf condition becomes a quadratic in the Hill term $h$,

$$2\hat{\alpha}^2 h^2 + \left(8\hat{\alpha} - \hat{\beta}\hat{k}\hat{\theta}\right) h + 8 = 0. \tag{25}$$

Solving Eq. (25) for $h$,

$$h = \frac{\left(\hat{\beta}\hat{k}\hat{\theta} - 8\hat{\alpha}\right) \pm \sqrt{\left(\hat{\beta}\hat{k}\hat{\theta} - 8\hat{\alpha}\right)^2 - 64\hat{\alpha}^2}}{4\hat{\alpha}^2}. \tag{26}$$

Since $h$ is a physical quantity, $h \in \mathbb{R}_{\geq 0}$, a Hopf bifurcation can occur only if this root is real, which requires the discriminant to be non-negative, $\left(\hat{\beta}\hat{k}\hat{\theta} - 8\hat{\alpha}\right)^2 \geq 64\hat{\alpha}^2$. Taking square roots and retaining the branch consistent with positive gain, $\hat{\beta}\hat{k}\hat{\theta} - 8\hat{\alpha} \geq 8\hat{\alpha}$, hence

$$\hat{\beta}\hat{k}\hat{\theta} \;\geq\; 16\,\hat{\alpha}. \tag{27}$$

Combining Eq. (27) with the parametric condition $\hat{r} < 1$ from Section B.3, we obtain a sufficient condition for the controller to destabilize the unique equilibrium of the self-inhibiting gene in the fast-sequestration regime. Since Section B.1 established that trajectories are bounded and the equilibrium is unique, instability of that equilibrium implies trajectories cannot settle to a fixed point and are driven into oscillations. We verify this claim through numerical simulations in the next section.

### C. *Numerical characterization of oscillations induced by the feedback controller*

Fig. 2–A compares the trajectories of the self-inhibiting gene in isolation (black) with the closed-loop system (orange), demonstrating that the IFFL controller induces sustained oscillations from zero initial conditions. The corresponding phase portrait (Fig. 2–B) shows a closed orbit, with the closed-loop equilibrium marked for reference. To validate the gain condition described by Eq. (27), Fig. 2-C shows a phase diagram in the $(\hat{\alpha}, \hat{\beta})$ plane, classifying each point by the eigenvalues of the full-system Jacobian at equilibrium. We note that the analytical condition (dashed line) coincides with the numerically identified boundary between oscillatory (orange) and non-oscillatory (grey) regions.

Moreover, to verify the range of $\hat{r}$ for which the controller is active, we simulated the closed-loop system across $\hat{r} \leq 1$ and slighly above. As shown in Fig. 2-D, the controller induces sustained oscillations for $\hat{r} \leq 1$, with amplitude decreasing as $\hat{r}$ approaches one. For $\hat{r} = 1.1$, the trajectories converge to the steady state of the isolated self-inhibiting gene, confirming that the controller exerts no action when $\hat{r} > 1$. Similarly, to the effect of finite sequestration, Fig. 2-E shows the trajectories at values of $\hat{\gamma}$ spanning two orders of magnitude around the nominal. Sustained oscillations for $\tau = 200$ persist across the upper range, and collapse to damped oscillations at the lowest values, which helps identifying a practical operating range over which the analytical conditions remain predictive.

We then tested the robustness of the controller-induced oscillations to perturbations in the process parameters. Fig. 3–A shows the closed-loop response when the production rate $(\hat{\alpha})$ and cooperativity $(m)$ are sequentially perturbed. The controller maintains sustained oscillations across all perturbed regimes, preserving the period (variations under 7%, while the amplitude shifts with the new parameter values. To

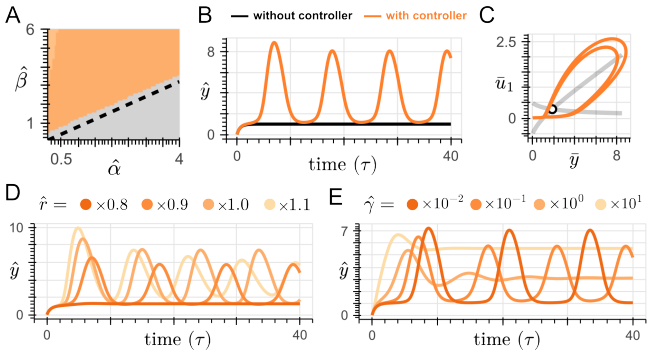


Fig. 2. **The controller induces sustained oscillations in the self-inhibiting gene.** (A) Trajectories of the isolated self-inhibiting gene (black) and the closed-loop system (orange), showing the emergence of oscillations under the IFFL controller from zero initial conditions. (B) Corresponding limit cycle in the $(\hat{y}, \hat{u}_1)$ phase plane under a simulation time of $\tau = 200$, with nullclines (grey) and the closed-loop equilibrium (black circle) marked for reference. (C) Phase diagram in the $(\hat{\alpha}, \hat{\beta})$ plane at $\hat{r} = 1$ and $\hat{\gamma} = 100$, classified by the eigenvalues of the full $4\times4$ Jacobian evaluated at the unique equilibrium. Dark orange indicates a complex-conjugate pair with positive real part; light orange indicates instability through a positive real eigenvalue with no unstable complex pair; and grey indicates a stable equilibrium. The dashed line shows the analytical gain condition from Eq. (27). (D) Closed-loop trajectories for $\hat{r} = \{0.8, 0.9, 1.0, 1.1\}$ at fixed $\hat{\beta} = 4$, varying $\hat{r}$ through $\hat{\rho}$. (E) Closed-loop trajectories for $\hat{\gamma} = \{1, 10, 100, 1000\}$ at nominal $\hat{r}$ and $\hat{\beta}$. The non–dimensionalized ODEs (Eq. 4–7) were used for these simulations, with the following nominal parameters: $\hat{\gamma} = 100$, $m = 1$, $\hat{k} = 2.5$, $\hat{\rho} = 25$, $\hat{\theta} = 10$.

systematically characterize this behavior, we swept $\hat{\alpha}$ and $m$ for increasing values of the gain $\hat{\beta}$, each satisfying the gain condition from Eq. (27). Fig. 3-B shows that the amplitude decreases with increasing $\hat{\alpha}$ and $m$, and is sensitive to the gain. In contrast, Fig. 3-C shows that the period is robust to both process perturbations and gain variations, remaining within a narrow band across all tested conditions.

### D. *Restoring sustained oscillations in a perturbed negative feedback oscillator*

To evaluate the controller on a more complex gene regulatory network, we consider a negative-feedback (NF) oscillator as the process. This architecture underlies many endogenous oscillators, including the NF-$\kappa$B signaling pathway [14] and the p53-Mdm2 circuit [15]. The NF oscillator can be modeled using the following chemical reactions:

$$\begin{aligned}
\emptyset \xrightarrow{\alpha p} M_Z, \quad & M_Z \xrightarrow{\delta} \emptyset, && \text{Transcription/Decay} \\
M_Z \xrightarrow{\kappa} M_Z + Z, \quad & Z \xrightarrow{\delta} \emptyset, && \text{Translation/Decay} \\
\emptyset \xrightarrow{\xi q} M_Y, \quad & M_Y \xrightarrow{\delta} \emptyset, && \text{Transcription/Decay} \\
M_Y \xrightarrow{\zeta} M_Y + Y, \quad & Y \xrightarrow{\delta} \emptyset, && \text{Translation/Decay}
\end{aligned} \tag{28}$$

where $p = K^m/(K^m + y^m)$ is the repression function and $q = z^m/(z^m + K^m)$ is the activation function. The $Y$ species serves as the feedback species to the IFFL controller, whose actuation on the process is given by:

$$U_1 \xrightarrow{\beta} U_1 + Y. \quad \text{(Controller Actuation)} \tag{29}$$

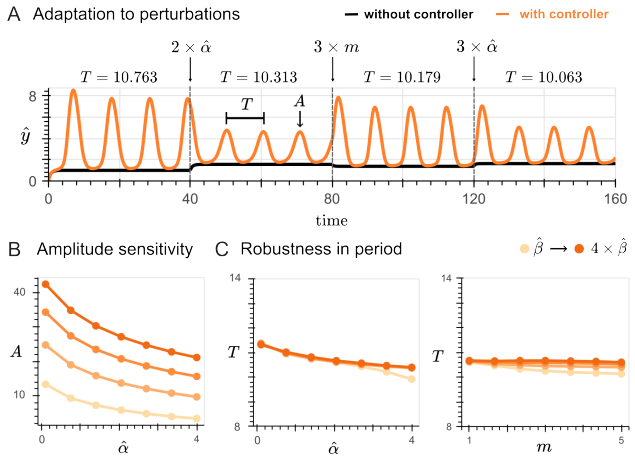


Fig. 3. **Robustness analysis.** (A) Closed-loop response under sequential perturbations to the process (dashed lines at $\tau = 40, 80$ and 120. The gain is fixed at $\hat{\beta} = 5$, which satisfies Eq. (27) for the largest deviation in $\hat{\alpha}$. (B) Amplitude $A$, measured as the mean peak-peak difference, as a function of $\hat{\alpha}$ for four values of $\hat{\beta}$ (light to dark), all satisfying the gain condition. (C) Period $T$, defined as the mean time between adjacent peaks, as a function of $\hat{\alpha}$ (left) and $m$ (right) for the same values of $\hat{\beta}$ as in (C). Nominal parameters as in Fig. 2.

We model the closed-loop system shown in Fig. 4–A using ODEs following the law of mass action. Applying the same non-dimensionalization as in Section 2-A, the resulting system is:

$$
\begin{aligned}
\frac{d\hat{m}_z}{d\tau} &= \hat{\alpha}\frac{1}{1+\hat{y}^m} - \hat{m}_z,\\
\frac{d\hat{z}}{d\tau} &= \hat{\kappa}\,\hat{m}_z - \hat{z},\\
\frac{d\hat{m}_y}{d\tau} &= \hat{\xi}\frac{\hat{z}^m}{1+\hat{z}^m} - \hat{m}_y,\\
\frac{d\hat{y}}{d\tau} &= \hat{\zeta}\,\hat{m}_y - \hat{y} + \hat{\beta}\,\hat{u}_1.\\
\frac{d\hat{u}_1}{d\tau} &= \hat{k}\,\hat{x} - \hat{\phi}\,\hat{u}_1 - \hat{\gamma}\,\hat{u}_1\,\hat{u}_2,\\
\frac{d\hat{u}_2}{d\tau} &= \hat{\rho}\frac{1}{1+\hat{y}^m} - \hat{\phi}\,\hat{u}_2 - \hat{\gamma}\,\hat{u}_1\,\hat{u}_2,\\
\frac{d\hat{x}}{d\tau} &= \hat{\theta}\frac{1}{1+\hat{y}^m} - \hat{\phi}\,\hat{x}.
\end{aligned}
\tag{30}
$$

The closed-loop system is shown in Fig. 4–A. We simulate the loss of periodicity by reducing the production rates and cooperativity of the NF oscillator, moving it from its oscillatory regime into a non-oscillatory one. Fig. 4–B (left) shows the resulting phase portrait without the controller, where the trajectory exhibits damped oscillations converging to a stable fixed point. Applying the IFFL controller with $\hat{r} \leq 1$ and a sufficiently high gain rescues the oscillatory behavior, as shown in Fig. 5–B (right), where a closed orbit emerges. Moreover, Fig. 4–C extends this analysis by showing the closed-loop response under sequential perturbations: a reduction in production rates, a decrease in cooperativity, and an increase in degradation rate. Without the controller, the NF oscillator (black) loses periodicity after the first perturbation, while the controlled system (orange) maintains

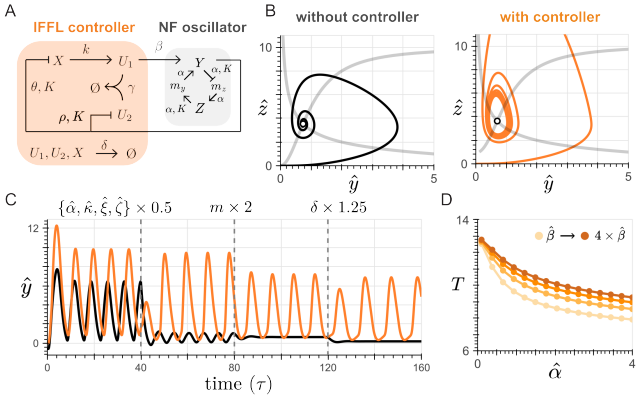


Fig. 4. **The IFFL controller induces sustained oscillations in the negative feedback (NF) oscillator in its non-oscillatory regime.** (A) Closed-loop diagram. (B) Phase portraits of the NF oscillator in the $(\hat{y}, \hat{z})$ plane: the uncontrolled system converging to a stable equilibrium (left, black), and the controlled system exhibiting a closed orbit (right, orange). Nullclines are shown in grey. (C) Time-domain response under sequential perturbations to the process: reduction in production rates, increase in cooperativity, and increase in degradation rate. Without the controller (black), the system loses periodicity after the first perturbation; with the controller (orange), sustained oscillations are maintained across all perturbed regimes. (D) Period $T$ as a function of $\hat{\alpha}$ for increasing values of $\hat{\beta}$ (light to dark). The non-dimensionalized ODEs (Eqs. 30) were used for these simulations, with the following nominal parameters: $m = 4$, $\hat{\alpha} = \hat{\xi} = \hat{\kappa} = \hat{\zeta} = 1/(\delta K)$, $\hat{k} = 2$, $\hat{\gamma} = 100$, $\hat{\theta} = 1/(\delta K)$, $\hat{\rho} = \hat{k}\hat{\theta}$, $\hat{\phi} = 1$, $\hat{\beta} = 1$. Perturbations in Panel C: production rates reduced by $0.5\times$, cooperativity increased to $m = 2$ (from $m = 4$), and degradation rate increased by $1.25\times$.

sustained oscillations across all perturbed regimes. Fig. 4–D characterizes the period of the resulting oscillations as a function of $\hat{\alpha}$ for increasing values of $\hat{\beta}$, confirming that the period remains robust to process perturbations across different gain values.

## III. Discussion

In this work, we designed a reference-free molecular feedback controller based on the IFFL motif that induces sustained oscillations in non-oscillating gene regulatory networks. Through a Hopf bifurcation analysis in the fast sequestration regime, we derived two design rules: a parametric condition on the controller's kinetic rates ($\hat{r} \leq 1$) and a gain condition ($\hat{\beta}\hat{k}\hat{\theta} \geq 16\hat{\alpha}$) that together are sufficient for sustained oscillations. Numerical simulations confirmed these conditions and demonstrated that the resulting oscillations are robust in period yet sensitive in amplitude to parametric perturbations.

These design rules admit a direct biological interpretation. The fast-sequestration assumption requires molecular components that bind strongly and stoichiometrically, a property well-characterized *in vivo* across a wide range of proteins and RNA molecules [11], [12]. The parametric condition $\hat{r} \leq 1$ requires the indirect production branch of the IFFL motif to dominate the direct one, while the gain condition requires the product of the actuation gain ($\hat{\beta}$) and the indirect branch's intermediate rates ($\hat{k}, \hat{\theta}$) to exceed the process production rate ($\hat{\alpha}$) by a sufficient margin. Both conditions can be tuned through standard synthetic-biology elements such as promoters, ribosome binding sites, and cis-regulatory

elements. Importantly, the relaxed nature of these conditions (any $\hat{r} < 1$ is admissible, and the gain has a broad operating range above its threshold) suggests that the controller is feasible with current toolkits.

Interestingly, the controller design has a connection to the minimal implementation of an adaptive controller. When analyzed in isolation under the fast-sequestration regime with $\hat{r} = 1$, the controller output approximates a filtered derivative of the process state [9]. Under this condition, the derivative action vanishes as the system approaches its steady state, which is a characteristic of adaptive controllers. While a formal proof of adaptiveness remains outside the scope of this work, this observation suggests that the same controller architecture could potentially be applied to stabilize an otherwise unstable biological system.

Finally, we acknowledge several limitations. The oscillatory conditions were derived for the self-inhibiting gene and explored numerically on the NF oscillator; extending the analytical framework to arbitrary processes is a natural next step, with tools from 2-cooperative systems theory [16] offering a promising direction. A related direction concerns systems that already oscillate, where the controller may either preserve the intrinsic dynamics of the process or impose its own oscillatory characteristics. Overall, this work emphasizes the design of genetic circuits based on dynamic properties rather than direct control of gene expression levels, and suggests that modular feedback strategies can offer a scalable alternative to the *de novo* design of genetic oscillators.

## APPENDIX

### A. Controller's nullclines equation

Analyzing the derivative with respect to $\hat{y}$ of Eq. (12) with the help of Wolfram Mathematica, we obtain

$$\frac{dN_1}{d\hat{y}} = -\frac{\hat{k}\hat{\theta}h}{\zeta\hat{\gamma}} - (1-\hat{r})\frac{\hat{k}\hat{\theta}h}{2}\left[1 + \frac{1}{\zeta}\left(\frac{\hat{k}\hat{\theta}(1-\hat{r})}{\hat{y}^m+1} - \frac{1}{\hat{\gamma}}\right)\right]$$

where $h = m\hat{y}^{m-1}/(1+\hat{y}^m)^2$ and

$$\zeta = \sqrt{\frac{4\hat{\gamma}\hat{k}\hat{\theta}(\hat{y}^m+1) + (\hat{\gamma}\hat{k}\hat{\theta}(\hat{r}-1) + \hat{y}^m + 1)^2}{\hat{\gamma}^2(\hat{y}^m+1)}}$$

which is $\zeta > 0$, $\forall \hat{r}$. Therefore, Eq. (12) describes a monotonically decreasing function for $\hat{r} < 1$, since $dN_1/d\hat{y} < 0$ for that $\hat{r}$ range, and approaches zero for increasing values of $\hat{\gamma}$ for $\hat{r} = 1$.

### B. Process' nullclines equation

Analyzing the derivative with respect to $\hat{y}$ of Eq. (13), we obtain,

$$\frac{dN_2}{d\hat{y}} = \frac{1}{\hat{\beta}} + \frac{\hat{\alpha}}{\hat{\beta}}\frac{m\hat{y}^{m-1}}{(1+\hat{y}^m)^2}$$

Therefore, Eq. (13) describes a monotonically increasing function, independent of the value of $\hat{r}$, since $dN_2/d\hat{y} > 0$.

## REFERENCES


[1] J. H. Levine, Y. Lin, and M. B. Elowitz, "Functional roles of pulsing in genetic circuits," *Science*, vol. 342, no. 6163, pp. 1193—1200, Dec. 2013. [Online]. Available: http://dx.doi.org/10.1126/science.1239999

[2] M. Nassan and A. Videnovic, "Circadian rhythms in neurodegenerative disorders," *Nature Reviews Neurology*, vol. 18, no. 1, pp. 7—-24, Nov. 2021. [Online]. Available: http://dx.doi.org/10.1038/s41582-021-00577-7

[3] Y. Lee, "Roles of circadian clocks in cancer pathogenesis and treatment," *Experimental & Molecular Medicine*, vol. 53, no. 10, pp. 1529—-1538, Oct. 2021. [Online]. Available: https://doi.org/10.1038/s12276-021-00681-0

[4] S. W. Sowa, M. Baldea, and L. M. Contreras, "Optimizing metabolite production using periodic oscillations," *PLoS Computational Biology*, vol. 10, no. 6, p. e1003658, Jun. 2014. [Online]. Available: http://dx.doi.org/10.1371/journal.pcbi.1003658

[5] Z. Zhou, Y. Liu, Y. Feng, S. Klepin, L. S. Tsimring, L. Pillus, J. Hasty, and N. Hao, "Engineering longevity—design of a synthetic gene oscillator to slow cellular aging," *Science*, vol. 380, no. 6643, pp. 376—381, Apr. 2023. [Online]. Available: http://dx.doi.org/10.1126/science.add7631

[6] M. Tomazou, M. Barahona, K. M. Polizzi, and G.-B. Stan, "Computational re-design of synthetic genetic oscillators for independent amplitude and frequency modulation," *Cell Systems*, vol. 6, no. 4, pp. 508–520.e5, Apr. 2018. [Online]. Available: http://dx.doi.org/10.1016/j.cels.2018.03.013

[7] C. Briat, A. Gupta, and M. Khammash, "Antithetic integral feedback ensures robust perfect adaptation in noisy biomolecular networks," *Cell Systems*, vol. 2, no. 1, pp. 15–26, 2016. [Online]. Available: http://dx.doi.org/10.1016/j.cels.2016.02.010

[8] M. Filo, S. Kumar, and M. Khammash, "A hierarchy of biomolecular proportional-integral-derivative feedback controllers for robust perfect adaptation and dynamic performance," *Nature Communications*, vol. 13, no. 1, Apr. 2022. [Online]. Available: http://dx.doi.org/10.1038/s41467-022-29640-7

[9] F. Britto Bisso, G. Giordano, and C. Cuba Samaniego, "Engineering cell fate with adaptive feedback control," *ACS Synthetic Biology*, vol. 14, no. 8, pp. 3163—-3176, Jul. 2025. [Online]. Available: http://dx.doi.org/10.1021/acssynbio.5c00299

[10] Y. Zhang, C. C. Samaniego, K. Carleton, Y. Qian, G. Giordano, and E. Franco, "Building molecular band-pass filters via molecular sequestration," in *2022 IEEE 61st Conference on Decision and Control (CDC)*. IEEE, Dec. 2022. [Online]. Available: http://dx.doi.org/10.1109/CDC51059.2022.9993401

[11] C. Briat, A. Gupta, and M. Khammash, "Antithetic proportional-integral feedback for reduced variance and improved control performance of stochastic reaction networks," *Journal of The Royal Society Interface*, vol. 15, no. 143, p. 20180079, 2018. [Online]. Available: https://doi.org/10.1098/rsif.2018.0079

[12] N. E. Buchler and M. Louis, "Molecular titration and ultrasensitivity in regulatory networks," *Journal of Molecular Biology*, vol. 384, no. 5, pp. 1106–1119, 2008. [Online]. Available: https://doi.org/10.1016/j.jmb.2008.09.079

[13] B. Novák and J. J. Tyson, "Design principles of biochemical oscillators," *Nature Reviews Molecular Cell Biology*, vol. 9, no. 12, pp. 981—-991, Oct. 2008. [Online]. Available: http://dx.doi.org/10.1038/nrm2530

[14] D. E. Nelson, A. E. C. Ihekwaba, M. Elliott, J. R. Johnson, C. A. Gibney, B. E. Foreman, G. Nelson, V. See, C. A. Horton, D. G. Spiller, S. W. Edwards, H. P. McDowell, J. F. Unitt, E. Sullivan, R. Grimley, N. Benson, D. Broomhead, D. B. Kell, and M. R. H. White, "Oscillations in NF-$\kappa$B signaling control the dynamics of gene expression," *Science*, vol. 306, no. 5696, pp. 704—-708, Oct. 2004. [Online]. Available: http://dx.doi.org/10.1126/science.1099962

[15] R. Lev Bar-Or, R. Maya, L. A. Segel, U. Alon, A. J. Levine, and M. Oren, "Generation of oscillations by the p53-mdm2 feedback loop: A theoretical and experimental study," *Proceedings of the National Academy of Sciences*, vol. 97, no. 21, pp. 11 250—11 255, Oct. 2000. [Online]. Available: http://dx.doi.org/10.1073/pnas.210171597

[16] R. Katz, G. Giordano, and M. Margaliot, "Instability of equilibrium and convergence to periodic orbits in strongly 2-cooperative systems," *Journal of Differential Equations*, vol. 444, p. 113651, Nov. 2025. [Online]. Available: http://dx.doi.org/10.1016/j.jde.2025.113651